Original Article

Corresponding author info

Corresponding Author:
David Bryant, University of Bradford, Richmond Road, Bradford, BD7 1DP, UK
Email: d.bryant@bradford.ac.uk

Simplified 3D Finite Element Hot Spotting Modelling of a Pin-Mounted Vented Brake Disc: An Investigation of Hot Spotting Determinants

[1]Tang, Jinghan[*]; [1]Bryant, David; [1]Qi, Hongsheng; [1]Whiteside, Ben; [1]Babenko, Max

[1]University of Bradford, Bradford, United Kingdom

Abstract

Hot spotting is a thermal localisation phenomenon in which multiple hot regions form on a brake disc surface during high energy and/or high speed braking events. As an undesired problem, hot spots can result in high order brake judder, audible drone and thermal cracking. This paper presents a finite element model for hot spot modelling which introduces the classical axisymmetric assumptions to the brake pad in 3D by scaling the material properties combined with a subroutine to simulate the heat generation instead of modelling the rotation of the brake pad. The results from the initial feasibility models showed significant improvement in computing efficiency with acceptable accuracy when compared to a traditional FE model without such simplifications. This method was then applied to the 3D simulation of hot spotting on a realistic ventilated brake disc/pad pair and the results showed good correlation with experiments. In order to improve the understanding of the hot spotting mechanism, parametric studies were performed including the effects of solid and ventilated disc geometry, rotational speed and energy, pins, disc run-out, and brake pad length. Based on the analysis of the results, it was identified that the vents and pins affected the hot spot distribution. Speed was shown to be more important on the hot spot generation time and distribution than either the pressure or total energy input. Brake disc run-out was shown to affect the magnitude of both hot spot temperature and height due to the non-linear relationship between local deformation, contact pressure and heat generation. Finally, increasing the brake pad length generated fewer hot spots but the temperature of each hot spot increased.

Keywords

Finite element method, brake disc, hot spotting, parametric study, thermo-elastic instability, temperature

Notations

c	J/(kg K)	Specific heat capacity
E	GPa	Young's modulus
E_i	MJ	Total energy input
K	W/m K	Thermal conductivity
P	bar	Brake line pressure
p	Pa	Contact pressure
p_t	%	Possibility of contact
p_w	kW	Brake power
q	W/m^2	Heat flux
R_i	m	Inner disc radius
R_o	m	Outer disc radius
t	s	Time
T	°C	Temperature
ΔT	°C	Thermal gradient of hot spot
T_h	mm	Brake disc thickness
x	mm	Circumferential brake disc coordinate
z	mm	Axial brake disc coordinate
Δz	mm	Height of hot spot
α	10^{-6}/K	Coefficient of thermal expansion
θ	°	Brake pad arc length
μ		Coefficient of friction
ν		Poisson's ratio
ρ	kg/m^3	Density
ω	rad/s	Angular disc velocity of real geometry

Abbreviations

2D	Two dimensional
3D	Three dimensional
DTV	Disc thickness variation
FE	Finite element
IBM	Inboard mean disc surface
IR	Infrared
OBM	Outboard mean disc surface
SI	International system of units
TEI	Thermo-elastic instability

1 Introduction

During heavy duty braking, a phenomenal amount of thermal energy is dissipated into a brake disc and can generate effects such as bulk deformation and thermal localisation phenomena at the brake disc surface [1]. Hot spots are thermal localisations that are circumferentially distributed on the brake disc rubbing surface with local temperature gradients. The primary concern of hot spots forming on a brake disc surface is that it can cause undesired vibration issues such as judder and audible drone due to brake disc

waviness distortion and surface ripples. The other undesired results of hot spotting include brake pair thermal fade, brake disc surface cracking and thermo-mechanical fatigue [2].

The typical hot spot trigger condition is high speed and medium to heavy duty brake applications. Thermo-elastic instability (TEI) theory [3, 4] explained the occurrence of hot spots as a complex thermo-mechanical localisation process which is triggered by an initial disturbance of contact pressure and subsequent uneven temperature, distortion, friction, and heat flux. Through analytical predictions, Dow and Burton [5] indicated that when the relative velocity of the contact pair exceeded a critical value and a certain critical brake disc temperature was reached, the brake will enter an unstable status and the uneven conditions of the brake disc will be exponentially amplified into hot spots. However, by comparing analytical and experimental results, it was found that the TEI theory overestimated the critical speed [6, 7]. In addition, Sardá et al. [8] argued the existence of critical speed through experimental hot spotting investigations for different braking energy, braking power, velocity and pressure. It was observed that the occurrence of hot spots was related to the energy input to the brake disc, which was also in agreement with other authors [9, 10].

According to the thermal imaging results of Sardá et al. [8], the distribution of hot spots showed an anti-symmetric mode between the inboard (closest to the knuckle) and outboard (wheel side) brake disc surfaces. It indicated that the waviness distortions of the brake disc were the determinant of the hot spots. Kao et al. and Fieldhouse et al. [11, 12] also observed the waviness distortions and argued that it was caused by thermal buckling of the brake disc due to high energy input. However, Fan et al. and Ma et al. [13, 14] analytically predicted the critical temperature of the high order brake disc waviness thermal buckling and found it was much greater than the common hot spotting temperature. In addition, Kasem et al. [10] argued that the hot spots formed first due to high thermal energy and subsequently triggered the brake disc waviness.

Moreover, there are some other possible determinants of hot spotting. Suryatama et al. [15] performed a 3D thermo-mechanical contact model with initial brake disc thickness variation (DTV) and the high temperature zones were found to be localised at the peaks of the brake disc surface ripples.

Fieldhouse et al. [16] indicated the vents of the ventilated brake disc caused uneven brake disc temperature distribution and the subsequent ripples due to uneven thermal expansion might be related to hot spotting. On the contrary, Kao et al. [17] argued that the vents can contribute to the brake disc heat dissipation and reduce the occurrence of hot spots. In addition, to reduce the effects of uneven heat dissipation to hot spotting, Bryant et al. [1] improved the vent design of a ventilated brake disc and significantly reduced the maximum brake disc temperature and the circumferential temperature variation.

According to analytical predictions, Lee et al. [18] suggested that the number of hot spots was related to the ratio of brake disc mean radius and the brake pad length. This was in agreement with the experiments of Sardá et al. [8] and numerical modelling of Panier et al. [19]. However, Cho et al. argued that the number of hot spot was determined by the periodic structural characteristics of the brake disc [7].

Since the analytical methods only provided the quasi-static solution and could not reproduce real geometry and complete boundary conditions of the brake, numerical methods became an effective tool to investigate hot spotting. As the discussion above demonstrates, the mechanism of hot spotting has not been fully understood and due to the complex mechanism and the high demand on computer resources, 2D in-plane and out-of-plane models have been focused on in previous research [19, 20, 21, 22,]. In order to reduce the model complicity and improve the computing efficiency, the brake pads were assumed to be axisymmetric and cover 360° of the contact surface [19, 20].

In order to improve cooling performance, ventilated brake discs are widely used on the front axles of passenger cars and increasingly more commonly on the rear axles of high performance vehicles. Meanwhile, the complex geometric and mechanical structure of a ventilated brake disc provides more challenges to the prediction of hot spotting, thus historically numerical models of hot spotting were mainly focused on solid brake discs [19, 23, 24].

To further the understanding of hot spotting, 3D modelling is a natural choice which can provide more realistic boundary conditions and represent more complicated brake disc structures than 2D simulations. However, the 3D simulations have rarely been focused upon in published research. By using a fully coupled transient thermo-mechanical finite element method, Jung et al. [23] simulated the hot spotting in 3D and validated the results through a dynamometer test. However, the hot spotting mechanism and characteristics were not further investigated.

This paper introduces an axisymmetric brake pad simplification method by applying a scaling factor into the material property and mechanical loading incorporated with a user subroutine to reproduce the frictional heat generation. The method facilitated the reduction in the computing time of 3D hot spotting models resulting in acceptable prediction accuracy. Therefore, this method enabled an efficient investigation of the important factors that affecting hot spotting to be performed including geometry factors, trigger conditions and brake pad length.

2 Experimental set-up and test programme

In order to provide a benchmark for the FE simulation, experiments were performed on a laboratory dynamometer to provide measured data to validate the FE models. The setup of the dynamometer and the transducers is shown in Figure 2.1. Three rubbing thermocouples were mounted on each friction ring at different rubbing radii; embedded thermocouples (±2.5°C accuracy) were mounted in each friction ring just below the rubbing surface at the mean rubbing radius; a pressure transducer measured brake line pressure, whilst synchronised capacitive non-contacting displacement transducers measured inboard and outboard brake disc axial displacement.

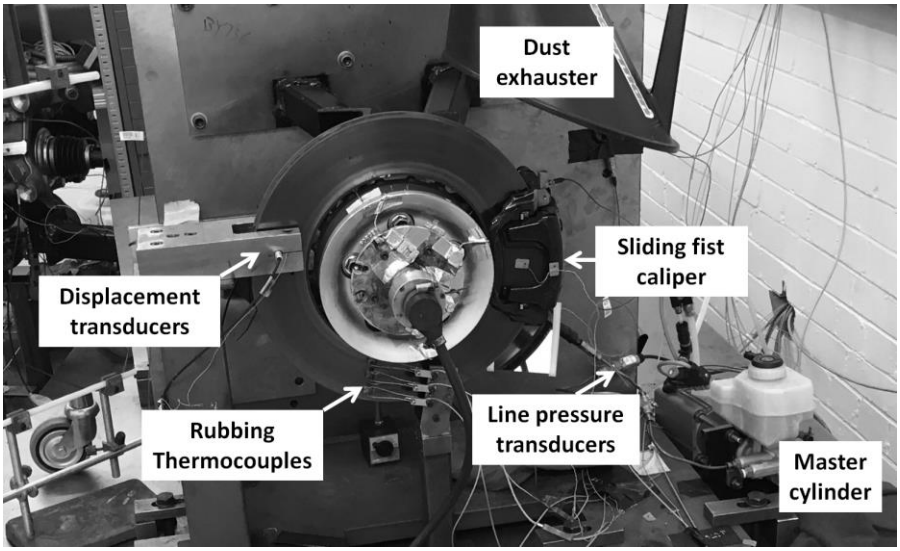

Figure 2.1 Arrangement of the dynamometer and associated transducers

The brake disc used for the test and simulation was a two piece pin-mounted ventilated brake disc using 17 pins to connect the grey cast iron friction ring to the aluminium top hat. There were 51 vents in total. The geometry and dimensions of the brake disc are shown in Figure 2.2. The brake pads comprised of semi-metallic friction material bonded to a steel backplate and were mounted in a single piston sliding fist type caliper.

To give a constant start temperature, the brake disc was pre-heated to 60°C. During the actual test, the brake was applied with constant 25.5bar line pressure at a constant brake disc speed of 976 rpm (~150km/h) for 24s (drag braking). The details of the braking parameters of the brake disc and pad are provided in Table 2.1. This formed the basis of the numerical study and generated suitable data to validate the models against.

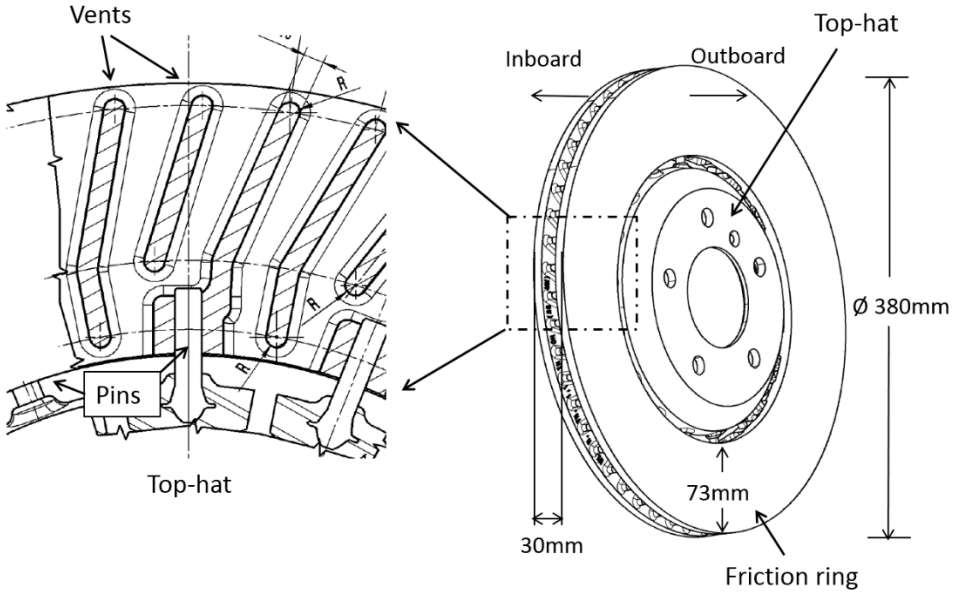

Figure 2.2 Cross section showing vent and pin geometry (left) and general brake disc geometry and basic dimensions (right)

Table 2.1 Braking data for both experiment and FE simulation

Braking operation parameters	
Nominal coefficient of friction, μ	0.38
Angular velocity, ω (rad/s)	102
Actuation pressure, P (bar)	25.5
Brake duration t (s)	24
Brake power P_w (kW)	51
Total energy input E_i (MJ)	1.2
Brake disc outer radius, R_o (mm)	190
Brake disc inner radius, R_i (mm)	117
Brake disc thickness, T_h (mm)	30
Brake pad arc length angle, θ(°)	30

3 Modelling assumptions and verification

3.1 Assumptions

In this study the assumption of an axisymmetric brake pad was inspired by Panier et al. and Zagrodzki et al. [19, 22], which regarded the brake pads as an equivalent friction material layer that circumferentially covered the brake disc surface. Zagrodzki et al. [22] only modelled a section of the disc in 2D equivalent to the length of the brake pad. To investigate the relationship between hot spot distribution with the brake disc waviness distortions, Panier et al. [19] modelled a solid brake disc and pad as beams with length equivalent to the circumference of the disc. To investigate the effects of vent pattern vs. brake pad length and brake disc run-out on hot spotting, it was necessary to model the full 3D brake disc in the present study together with a 3D axisymmetric brake pad. The 3D axisymmetric pad would allow the effects of pad thermal expansion and axial temperature distribution to be modelled, thus influencing contact pressure distribution.

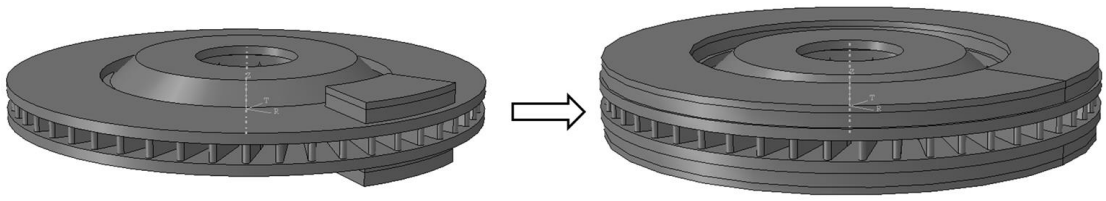

Figure 3.1 Real brake disc and friction material (lining) and back-plate model (left) and axisymmetric brake pad model with lining and back-plate (right)

Figure 3.1 shows the real brake geometry with finite length brake pad and the axisymmetric brake pad model. To convert the rotating 3D brake disc and stationary brake pad with finite arc length to the axisymmetric brake pad approximation, some assumptions were made and some conditions needed to be satisfied.

Assumptions:

i. Within one disc revolution, the nodal temperature variation due to rotational periodic heating is assumed to be negligible under high rotational velocity. In the 3D rotation model, the heating process can be regarded as a fast moving heat source rotating in the circumferential direction of the brake disc surface. For a given point on the brake disc surface, the heating procedure is composed by both heating and cooling phases during each brake disc revolution (illustrated by Figure 3.2). Thus, the circumferential temperature difference on the brake disc surface of the axisymmetric model is inevitable. However, the circumferential temperature difference is assumed to be negligible compared with the bulk brake disc temperature evolution when the rotation speed is high as in this example. Heat flux was also assumed to increase linearly with increasing radius for a given constant contact pressure.

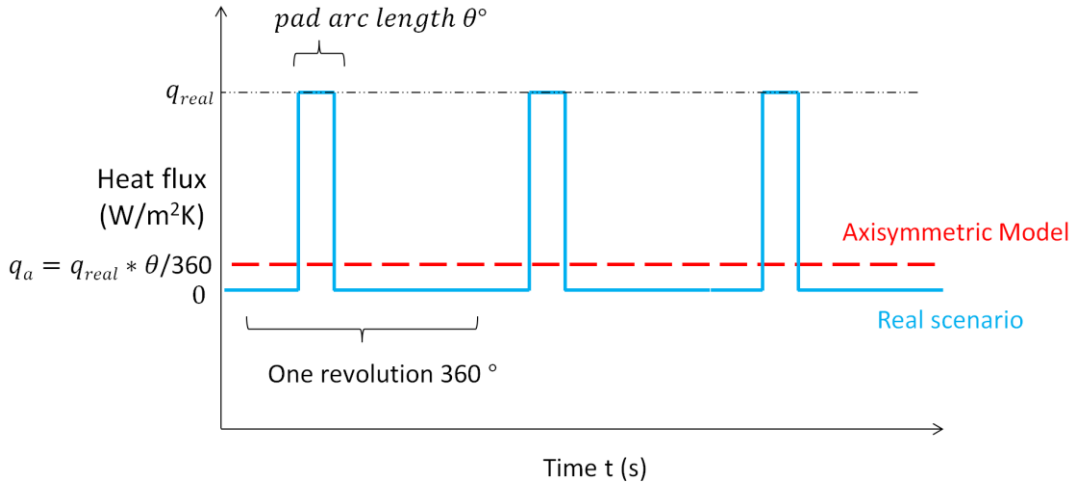

Figure 3.2 Representation of ideal heat generation time series at a fixed brake disc surface node for both periodic heating mode (real scenario) and continuous heating mode (axisymmetric approximation) with uniform constant contact pressure (Note: subscript '$_a$' indicates axisymmetric model and '$_{real}$' indicates the real model)

ii. There is no relative rotation between the axisymmetric brake pad and the brake disc, therefore the circumferential friction force was not considered. According to literature [5, 19, 22], the traction force does not significantly affect the prediction of hot spots.

Based on the assumptions, the results of the simplified model should satisfy the following conditions:

i. Comparable brake disc temperature distribution. To reproduce the hot spotting generation in the axisymmetric brake pad model, the temperature distribution of the simplified model should be comparable with the realistic scenario in order to achieve same heat partition ratio and thermo-elastic deformation.

ii. Identical total heat generation. In the previous heat transfer studies of brake disc brake assemblies, the identical total heat generation is the most frequently used assumption. In order to achieve identical thermal deformation of the brake disc, the heat that goes into the brake disc should be essentially identical.

iii. Identical total mechanical loading. This assumption is made to keep the total clamping force and the total strain energy identical.

iv. Comparable heat flux and contact pressure distribution. In order to achieve a comparable temperature field, the heat flux distribution should be comparable in both models. As the heat flux is determined by contact pressure, comparable contact pressure distribution should also be satisfied.

v. Identical strain energy on the brake disc. To achieve comparable contact pressure distribution, the total strain energy should be identical. The strain energy density distribution in both cases should also be the same.

3.2 Scaling factors

Since the volume of the brake pad and contact area were increased in the axisymmetric brake pad model, to satisfy the above assumptions and conditions, the loading condition and material properties of the brake pad had to be scaled [20]. From a probability density point of view, the probability in the time domain is $p_t = \theta/360$ for a discreet point on the brake disc to access the heat flux or mechanical load from the real brake pad, where θ is the brake pad length. To satisfy the comparable friction effects as discussed in section 3.1, scale factors were applied to the parameters listed in Table 3.1. The details of the calculations can be found in [27].

Table 3.1 list of the scaled material and brake parameters

Parameter	Original	Scaled	Scale factor
Thermal conductivity	k_{real}	$k_a = k_{real} * \theta/360$	$\theta/360$
Density	ρ_{real}	$\rho_a = \rho_{real} * \theta/360$	$\theta/360$
Young's modulus	E_{real}	$E_a = E_{real} * \theta/360$	$\theta/360$
Contact pressure	p_a	$p_a = p_{\text{real}} * \theta/360$	$\theta/360$

Note: subscript '$_a$' indicates axisymmetric model and '$_{real}$' indicates the real model.

3.2 Comparison of numerical models under different assumptions

In order to verify the scaling factor method, three finite element models under different assumptions were performed as shown in Figure 3.3. The geometry of the models were based on a reduced scale brake system in order to reduce the total number of elements since the computing time for a 3D thermo-mechanical contact model with rotation is considerable. For model A, the brake pad length was finite (30°) whereas the brake pads of model B and C were 3D modelled where the axisymmetric assumption were used for the brake lining friction material. The brake discs of model A and B were rotating, while stationary in model C. The comparison between model A and B was expected to reveal the accuracy of the axisymmetric brake pad simplification. The purpose of comparing models B and C was to verify if the modelling of rotation (i.e. traction forces) can affect the accuracy of the results. The temperature-independent material properties (using a

simplified isotropic assumption at room temperature) and braking parameters were provided by Table 3.2 and Table 3.3. In Table 3.2, the scaled material properties were applied to model B and C whereas the original data were used in model A. In order to verify the variability between the results for different models, the frictional heat generation and coefficient of thermal expansion were both exaggerated by 10 times which was presumed to amplify the variability (Note: the coefficient of thermal expansion shown in Table 3.2 does not include this exaggeration). In model C, since there was no relative motion between the contacts, the frictional heat generation was defined using ABAQUS user subroutine FRIC. The nodal heat flux generation was calculated and updated at each time increment based on the predefined coefficient of friction, radius dependent nodal velocity and the nodal contact pressure retrieved from the simulation results at the same time increment. The heat generation was assumed to be equally generated at the brake disc and pad and the actual heat partition was determined by the thermal contact conductance ($30kW/m^2K$) at the interface which was set as a pressure and clearance dependent variable.

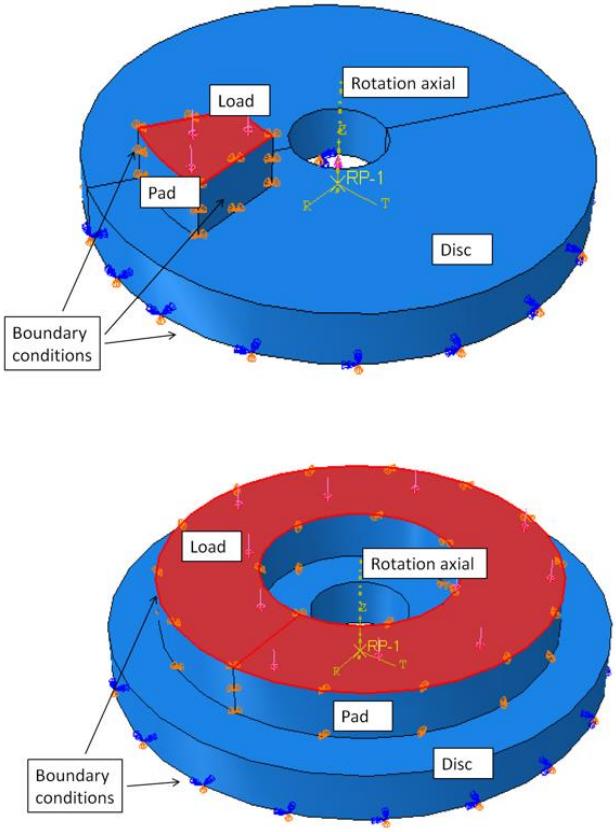

Model A: rotating brake disc and stationary brake pad

Model B: rotating brake disc and stationary axisymmetric brake pad

Model C: stationary brake disc and stationary axisymmetric brake pad with subroutine

Figure 3.3 Scale brake models for verification of the assumptions with boundary conditions indicated. Top: scale rotating disc (Model A); bottom: axisymmetric brake pad with either rotating disc (Model B) or stationary disc (Model C).

Table 3.2 Material properties before and after scaling for FE simulations

Material properties	Disc	Pad	Scaled pad	Back-plate	Scaled back-plate	Top hat	Pins
Thermal conductivity, k (W/(m K))	48	0.5	0.042	50	4.2	113	17
Density, ρ (kg/m^3)	7200	1250	104.2	7800	650	2680	7800
Elastic modulus, E (GPa)	100	0.7	0.058	210	17.5	71	210
Poisson's ratio, v	0.25	0.25	0.25	0.3	0.3	0.33	0.34
Coefficient of Thermal expansion, α (10^{-6}/K)	10	10	10	11	11	21	11
Specific heat capacity c (J/(kg K))	480	1000	1000	500	500	880	500

Source of data: industry, measurements and literature [21, 25]

Table 3.3 Brake data for the scale brake models

Braking operation parameters	
Nominal coefficient of friction, μ	0.38
Angular velocity, ω (rad/s)	30
Actuation pressure, P (bar)	10
Brake disc outer radius, R_o (mm)	50
Brake disc inner radius, R_i (mm)	10
Brake disc thickness, T_h (mm)	10
Brake pad arc length angle, θ (°)	30

Figure 3.4 and 3.5 shows the comparisons of the temperature and axial displacement fields at the end of the simulations (5s). The results suggested that the average temperature field and displacement distributions for all three scale models were similar. Though there were circumferential peak temperature and displacement variations (~ 400 °C or ~100μm) due to the periodic heating in the rotating brake disc model generating higher surface temperatures at the trailing side of the pad, the average temperatures (351°C, 369°C and 368°C) and displacement (199μm, 213μm and 212μm) of the rubbing surfaces were similar. Regarding the maximum brake disc temperature and displacement, Figure 3.6 and 3.7 provide the time-series plot of a single node on the mean rubbing radius. It was clear that the periodic heating of Model A provided similar average temperature and displacement evolutions to the axisymmetric brake pad models. Since the axisymmetric brake pads were used for model B & C, the temperature or heat generation can be regarded as being averaged in the time domain. Therefore, the maximum temperature predicted in models B & C was an underestimation of the maximum temperature of model A; this is a limitation of the axisymmetric modelling technique. Moreover, Model B and C achieved similar maximum temperature (1125°C and 1090°C) and displacement (584μm and 579μm) at 5s respectively. These values and the temperature fluctuation in model A are unrealistically high compared with common brakes which is a result of the exaggeration the of frictional heat generation effect, however they help to amplify some of the effects being investigated. It should

be noted that when the heat generation was not exaggerated the temperature variations between each model were much smaller and peak temperatures more realistic (not presented here). Therefore, the comparisons revealed that the axisymmetric brake pad and no traction behaviour assumptions can provide acceptable results (~5% and ~7% error in average surface temperature and axial displacement when compared with the real brake pad geometry Model A) by implementing the scaling factor method and user subroutine.

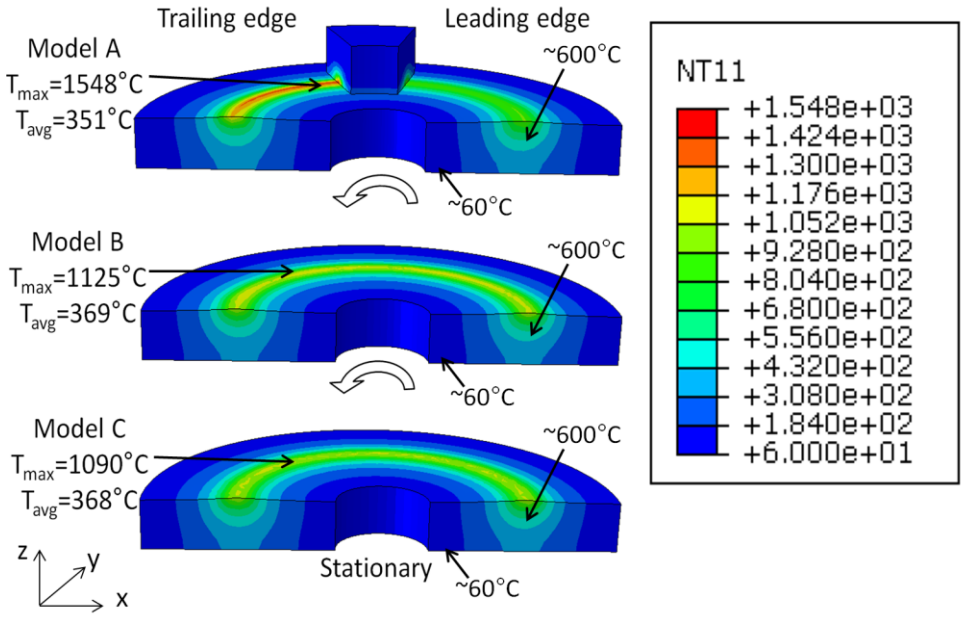

Figure 3.4 Temperature fields and maximum brake disc temperature (°C) for the three scale models at 5s

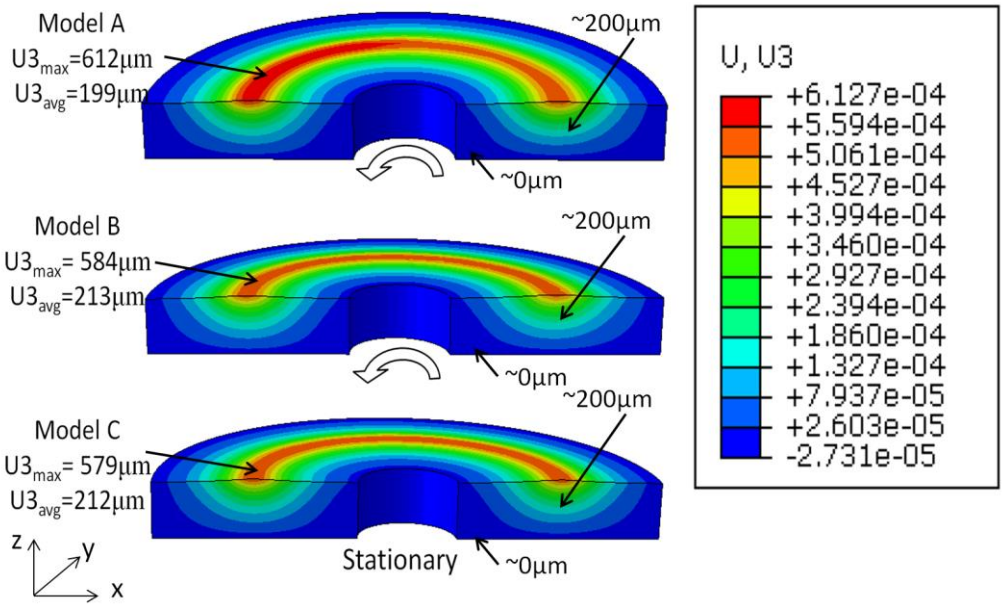

Figure 3.5 Displacement field with the colours indicating the maximum axial (z-direction) brake disc displacement (m) for the three scale models at 5s

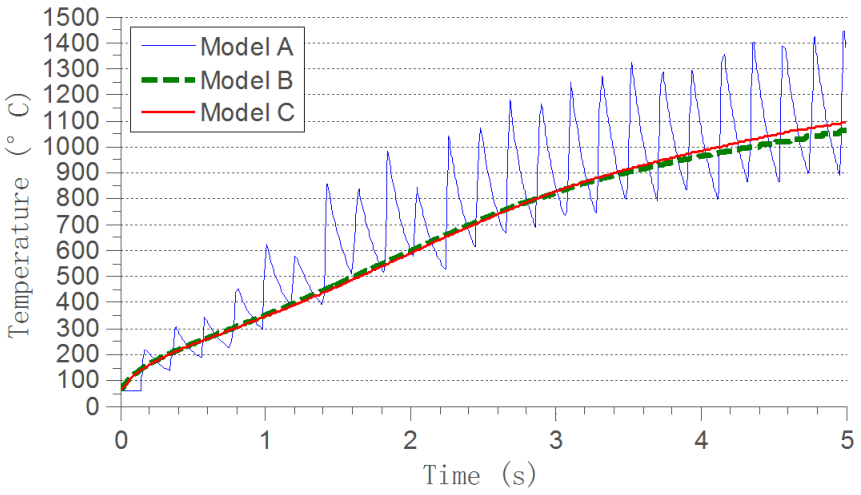

Figure 3.6 Brake disc temperature evolution of a single surface node at the mean rubbing radius; comparison between periodic heating (model A) and continuous heating in (axisymmetric models B and C)

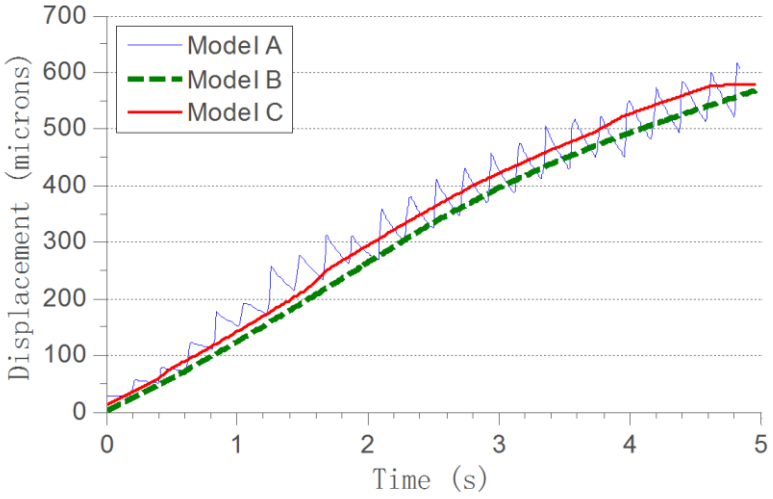

Figure 3.7 Evolution of brake disc displacement of a single surface node at the mean rubbing radius; comparison between periodic heating (model A) and continuous heating (axisymmetric models B and C)

The most significant aim of the axisymmetric model was to improve the computing efficiency with acceptable temperature and displacement results. Thus a comparison of the element number and computing time is provided in Table 3.4. In terms of element number, model B and C had the largest number of elements (16380 elements); this was because the axisymmetric brake pad had greater volume. Though both model A and B incorporated the rotation of the brake disc and frictional heat generation and had comparable results, model B took 5 times longer to solve due to the more complex contact interactions. However, the computing time of model C was significantly reduced, when compared with the rotating brake disc models A and B, and maintained comparable results. This can be explained by the elimination of the computing of rotation and shear traction behaviours. Thus, it is clear that the axisymmetric 3D brake pad assumption cannot improve the computing performance directly; the removal of

rotation effects is the main contributor to computing performance. Therefore, the axisymmetric brake pad assumption should be applied in conjunction with the removal of rotation.

Table 3.4 Number of elements in the scale 3D FE models and computing time

Model	Total element number	Computing time
A	9750	10hour 1min
B	16380	50 hour 33min
C	16380	1hour 16min

In summary, the results from the feasibility study suggested that the axisymmetric brake pad models with heating defined by a subroutine (to replace the brake disc rotation) were the most time efficient method to obtain similar temperature and displacement field predictions.

4 3D ventilated brake disc hot spotting modelling and results

4.1 FE model mesh and boundary conditions

The axisymmetric brake pad assumption and stationary brake disc assumptions were implemented in the full scale ventilated brake disc FE model. As shown in Figure 4.1, the axisymmetric assumption was applied to the brake pad and the detailed structure of the brake disc such as vents, pins and top hat was retained. The scaled material properties of the brake pad and loading conditions are shown in Table 3.2 and Table 2.1. Since only one drag brake application was simulated with no cooling phase, the permanent thermo-plastic effects were considered as insignificant. Thus the plasticity of the material properties was not incorporated into the model.

Regarding the boundary conditions as shown in Figure 4.1, the back-plates were constrained in the radial and circumferential directions (U1=U2=0) so that the brake pads were free to move in the axial direction and the friction material itself could thermally expand in the radial, axial and circumferential directions. The initial temperature was set to 60°C throughout the model which was consistent with the experiments. The brake disc was constrained at the outboard face of the top-hat. Uniform pressure was applied on the inboard and outboard back-plates according to the scaling factor from Table 3.1. Convective heat transfer coefficient on the brake disc surface was set to 70W/m^{2}K and the vents were 100W/m^{2}K based on experimental estimation. Radiation was considered small and neglected in this study. Coupled temperature displacement elements, C3D8T, were used for brake disc rotor surfaces and C3D4T for vents, pins and top-hat. The global element size was ~4.5mm. Since the deflection/distortion of thermal localisations are generally much smaller than the brake disc thickness, the mesh of the rotor surfaces were refined to ~1.5mm (see Figure 4.1) in order to achieve more accurate results. The frictional heat generation was defined by user subroutine FRIC to compensate for the absence of rotation.

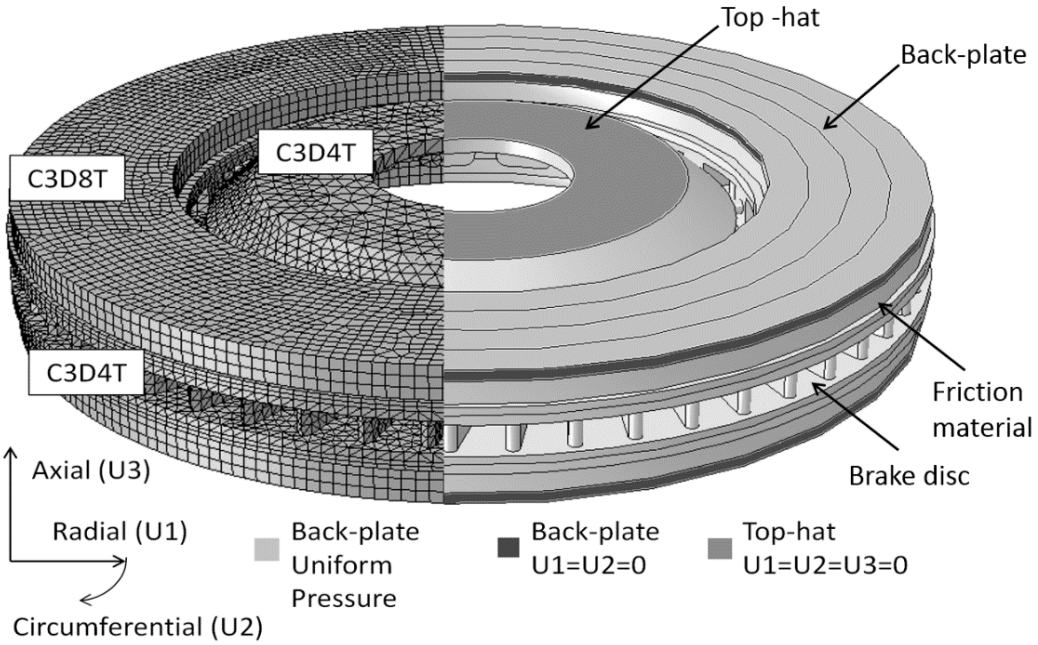

Figure 4.1 Mesh (left half) and boundary conditions (right half) of the pin-mounted ventilated brake disc brake FE model

4.2 Results and validation

The outboard temperature field of the brake disc surface showing hot spot developments at different time increments is shown in Figure 4.2. It can be seen that a hot band was initiated at the outer radius of the brake disc surface at 6s. A circumferential temperature difference indicating the onset of hot spotting was observed at 15s. At the end of the braking event (t=24s), 17 hot spots had clearly developed which matched the number of pins and was one third of the number of vents. The maximum brake disc surface temperature reached was 565°C, and the radial temperature difference between hot spots and surrounding brake disc surface was over 150°C. Regarding the temperature distribution between the inboard and outboard brake disc surface, an anti-symmetric distribution was observed in Figure 4.3, which is in agreement with literature [8, 9, 11, 12]. Figure 4.4 shows the axial brake disc deformation, stress and contact pressure distribution on the outboard surface in SI units at 24s. The displacement and contact pressure distributions matched with the temperature distribution as 17 ripples of surface deflections and 17 high pressure contact zones were observed. Such correlation revealed the significant contribution to hot spotting in terms of the interactions of uneven contact pressure, uneven temperature and uneven displacement. In addition, the stress field in Figure 4.4 illustrated the high stress concentration on the mean rubbing radius of the brake disc surface during hot spotting. Meanwhile, the pins between the friction ring and the top-hat showed high stress indicating their potential interaction in constraining the brake disc deformation.

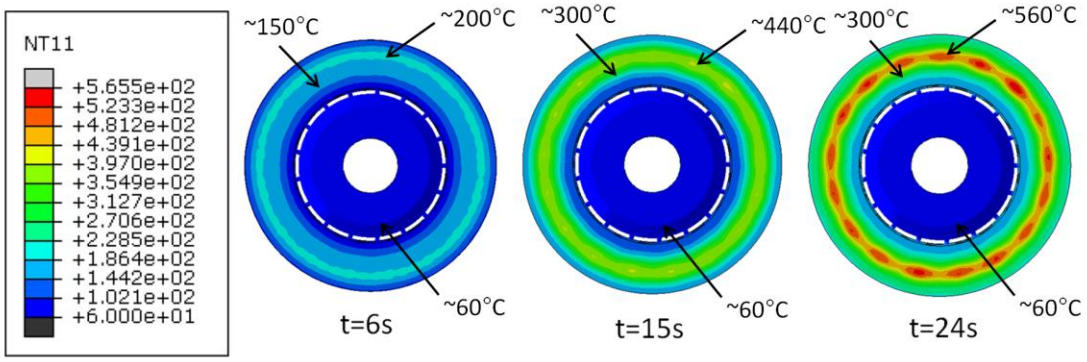

Figure 4.2 FE results showing the surface temperature distribution (°C) and hot spot development at the outboard disc surface

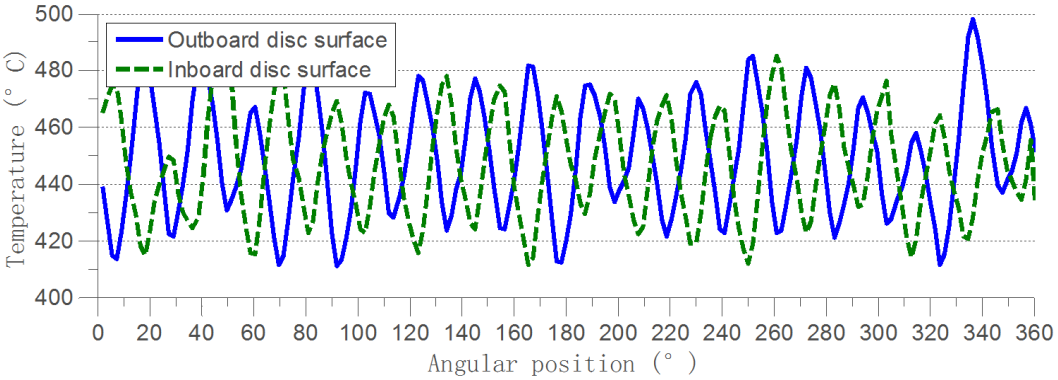

Figure 4.3 Brake disc mean radius surface temperature distribution extracted from the FE simulation at the end of the brake event (24s)

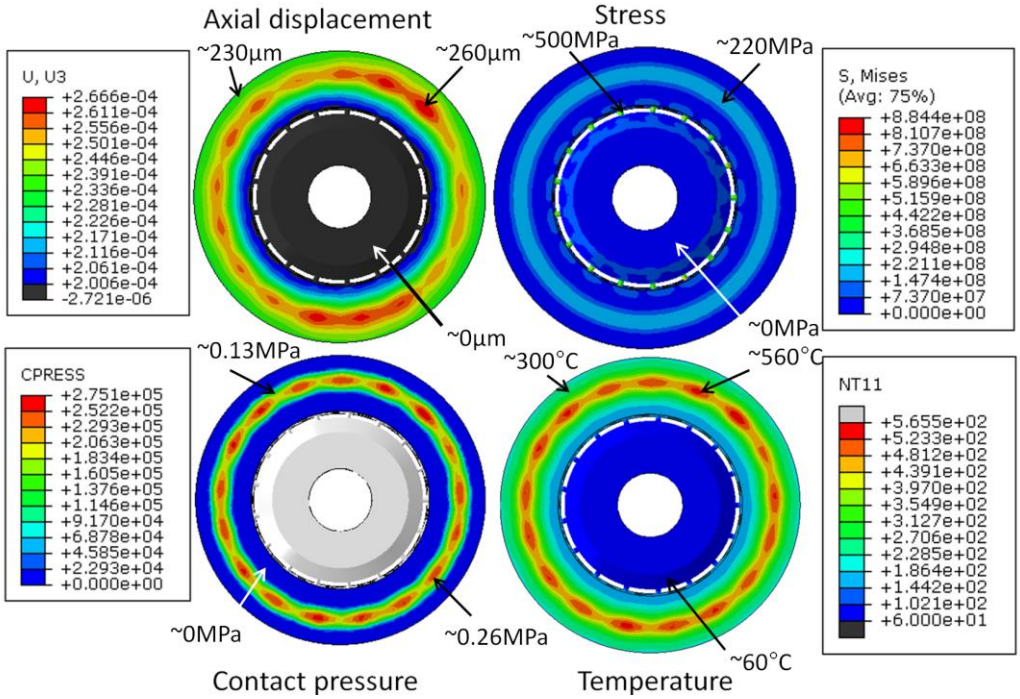

Figure 4.4 FE results showing axial displacement (m), stress (Pa), contact pressure (Pa) and temperature (°C) distributions of the outboard disc surface at 24s

The comparison between experimental temperature evolution (measured via the rubbing thermocouple at the mean radius) and the simulation results (fixed node at the mean rubbing radius) at the outboard mean rubbing radius is provided in Figure 4.5. It illustrates that the numerical maximum temperature overestimation (510°C vs. 460°C) was ~11% which is acceptable considering the simplifications and assumptions used for the FE model (absence of temperature-dependent material properties, constant coefficient of friction, no wear and no thermo-plastic effects), and likely difference between radial hot band position and rubbing thermocouple location.

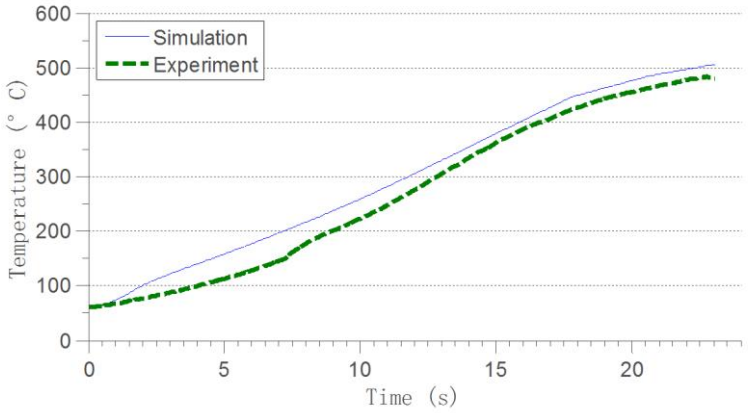

Figure 4.5 Brake disc mean radius temperature at the outboard surface; comparison between experiment (mean radius rubbing thermocouple) and FE simulation (mean radius nodal temperature)

The temperature distribution was also obtained by infrared thermal imaging in the experimental studies using a high speed thermal camera (FLIR X6540sc operating at 1kHz in windowed mode) with emissivity dynamically calibrated from thermocouple data at 3 different locations (within range from ~0.2 to ~0.6). The comparison between thermal image and simulation is shown in Figure 4.6, which revealed good correlation in terms of radial and circumferential distribution and the magnitude of the temperature gradients.

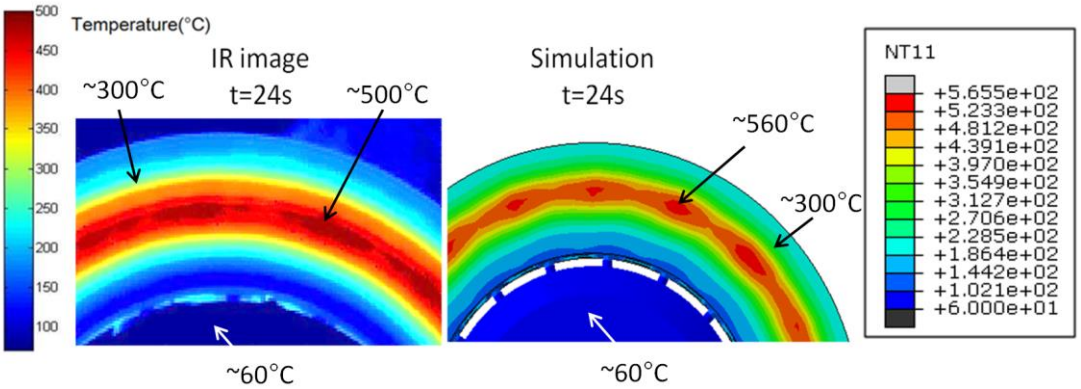

Figure 4.6 Thermal imaging (IR camera) of the brake disc outboard surface (left) and simulation results (right; °C) 24 seconds into the braking event

In the experiment, the outboard and inboard brake disc distortion were measured using displacement traducers with high sample rate (50kHz) that enabled the measurement of

the brake disc surface ripples due to hot spotting. According to Figure 4.4, the height of the hot spots predicted in the axisymmetric model was ~5 to 15 µm which matched well with the experimental measurements (~5 to 15 µm) as shown in Figure 4.7. In addition, Figure 4.7 showed a predominant second order brake disc run-out and the 17th order brake disc thickness variation due to hot spotting can also be observed. The run-out plots also validated that the hot spots were anti-symmetrically distributed since the inboard and outboard brake disc surface high order ripples showed the same waviness shape. Moreover, the line pressure also showed a 17th order variation (~0.03MPa) which demonstrated the judder effects due to hot spots.

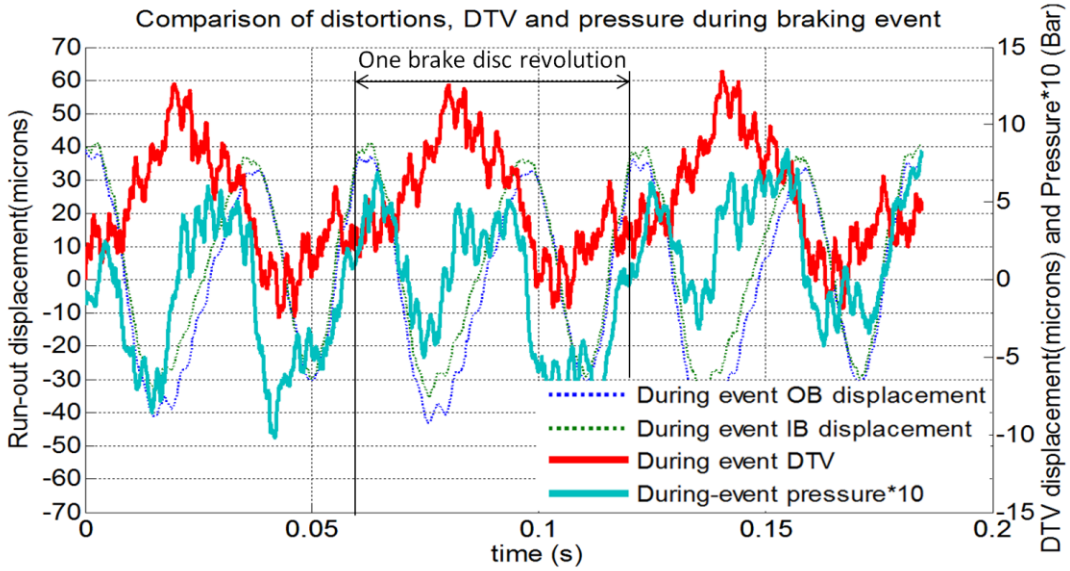

Figure 4.7 Experimental measurements of inboard and outboard brake disc surface displacement, brake disc thickness variation and line pressure variation in three brake disc revolutions at the end of the braking event (brake still applied)

5 Parametric studies

As identified in the introduction, the mechanism of hot spotting is still not fully understood. The theoretical debates mainly concentrated on the trigger conditions of hot spots (critical speed vs. energy input) [4, 5, 9, 10], effects of brake disc structural characteristics (vents, pins, solid or ventilated) [1, 16, 17], initial brake disc waviness [15] and brake pad length [7, 8, 18, 19]. Therefore, in order to investigate the effects of the determinants on hot spotting, a parametric study was performed based on the 3D model presented in section 4.

5.1 Solid vs. ventilated brake disc

As discussed, the simulation of hot spotting of ventilated brake discs has been only focused on by fewer authors [23, 28] in published literature compared to that of solid brake discs. Therefore, solid brake disc models using the modified real brake geometry were generated using the same axisymmetric brake pad method in order to investigate the effects of vents. According to [26], to achieve a like-for-like comparison in terms of thermal mass (i.e. equivalent temperature rise), the effective solid rotor thickness should be three times that of a single rotor face thickness on the ventilated brake disc.

As shown by Figure 5.1, the rotor face thickness was 9mm, so that the effective solid rotor thickness was 27mm. Moreover, a twice rotor face thickness solid brake disc model was also constructed to investigate the effects of rotor thickness on hot spotting.

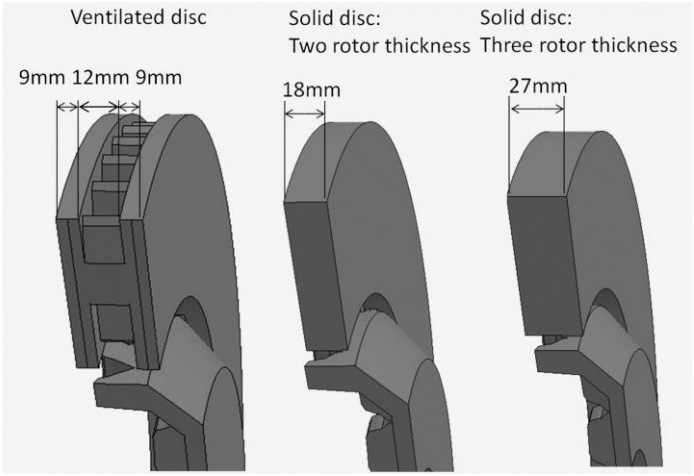

Figure 5.1 Thickness of the ventilated brake disc and solid brake discs for the parametric FE study

The temperature distributions of the ventilated, 18mm solid and 27mm solid models are shown in Figure 5.2. It can be seen that there were 17, 12 and 14 hot spots respectively and the maximum surface temperatures were 589°C, 689°C and 635°C respectively. The results implied that fewer hot spots were generated in the solid brake discs and the thicker brake disc generated more hot spots but lower maximum temperature and circumferential temperature gradient. Therefore, it is clear that the periodic vent and pin structure of the ventilated brake disc redistributed the braking energy into 17 sections and resulting 17 minor hot spots when compared with the solid brake disc. Moreover, it should be also noted that the distribution of hot spots were also anti-symmetric in the two solid models.

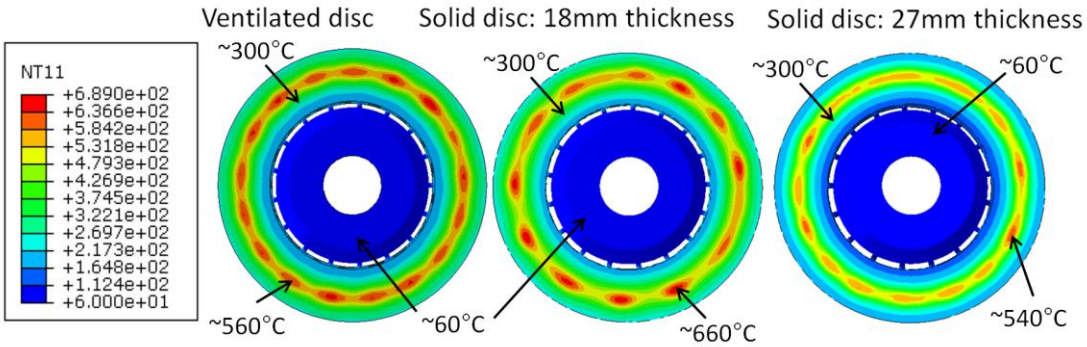

Figure 5.2 FE results showing the outboard brake disc surface temperature distributions (°C) of different brake disc structures (ventilated vs. solid) at 24s

5.2 Trigger condition for solid brake disc hot spotting

Since the debate about the trigger condition of hot spotting was focused on velocity and energy input, nine drag brake models under different speed and load were performed to

investigate their effects. The details of the models are listed in Table 5.1. It can be seen that three velocities and three brake line pressure were selected which provided nine combinations. The speed and pressure varied between 2/3, 1 and 3/2 times of the standard condition performed in section 4. Therefore, various braking power and energy input under identical speeds or pressures were able to be compared. In order to compare the hot spotting phenomena at the same braking time or same energy input, the brake duration was set to be a function of brake power. 18mm solid brake discs were selected in this study in order to remove the effects of periodic rotor structure, i.e. vent pattern.

Table 5.1 Loading conditions of the nine FE models for the hot spot trigger condition investigation

Model ID	Brake disc speed (rev/min)	Vehicle speed (km/h)	Pressure (Bar)	Power (kW)	Brake duration (s)	Energy at 24s (MJ)	Time at which identical energy input achieved (s)
1	654	100	17.1	22.9	54	0.6	54
2	654	100	25.5	34.2	36	0.8	36
3	654	100	38.3	51.3	24	1.2	24
4	976	150	17.1	34.2	36	0.8	36
5	976	150	25.5	51.0	24	1.2	24
6	976	150	38.3	76.6	24	1.8	16
7	1460	225	17.1	51.2	24	1.2	24
8	1460	225	25.5	76.3	24	1.8	16
9	1460	225	38.3	114.6	24	2.8	11

Figure 5.3 shows the outboard brake disc temperature distribution of the models at the same braking time (24s). The maximum temperature and time are given for each plot. The figure illustrated that at the same speed, the maximum temperature increased with increasing pressure but the hot spot distributions were similar. At the lowest speed (654rev/min) in the study, only hot bands appeared. At 976rev/min 12 hot spots were equally distributed on the mean brake disc rubbing radius. Since no wear and temperature dependent material property effects were considered in the models, the results of model 7 to 9 at 1460rev/min were discarded as the maximum hot spot temperature predicted was unrealistically high. In addition, when both speed and pressure were increased, the maximum temperature increased with the total energy input. But for identical brake power (Model 4 vs. 2 and 5 vs. 3); the high speed low pressure models provided apparent hot spotting compared with the low speed high pressure models. Therefore, the comparison at the same braking time (24s) illustrated that the brake disc speed is more important than braking power and pressure in determining the hot spot distribution.

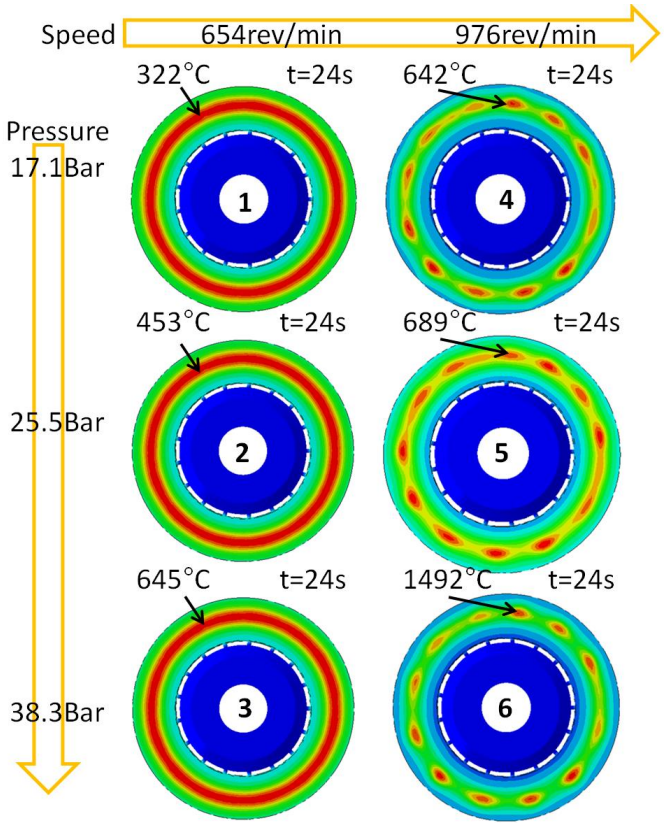

Figure 5.3 Outboard brake disc surface hot spot distribution and maximum brake disc temperature (indicated on figure) of the FE model at 24s at different speeds and loads

Figure 5.4 provides a comparison for different speed and pressure at identical total energy input into the brake disc (by varying the brake duration). It is clear that at the same energy level, the hot spot distributions were affected by speed and pressure. At the lowest speed in this study (654rev/min), there was no hot spotting, but the maximum temperature was increased with the pressure. At 976rev/min, the hot spots were more distinguished and with decreasing pressure, more heat was concentrated into each hot spot giving greater temperature.

Regarding the occurrence of hot spots, Figure 5.5 provides the temperature distribution and the time at which the hot spots became apparent. It can be seen that with differing pressure, there was no change in the hot spot or hot band distribution or the time at which the hot spots appeared. The only difference is that the maximum temperature increased with increasing pressure. In addition, 12 hot spots appeared at 17s at 976rev/min, whilst 12 more distinguished hot spots can be observed at 7s at 1460rpm. Therefore, it is clear that the hot spot distribution and trigger time were affected by the brake disc speed; greater the speed, lower the trigger time with clearer hot spots.

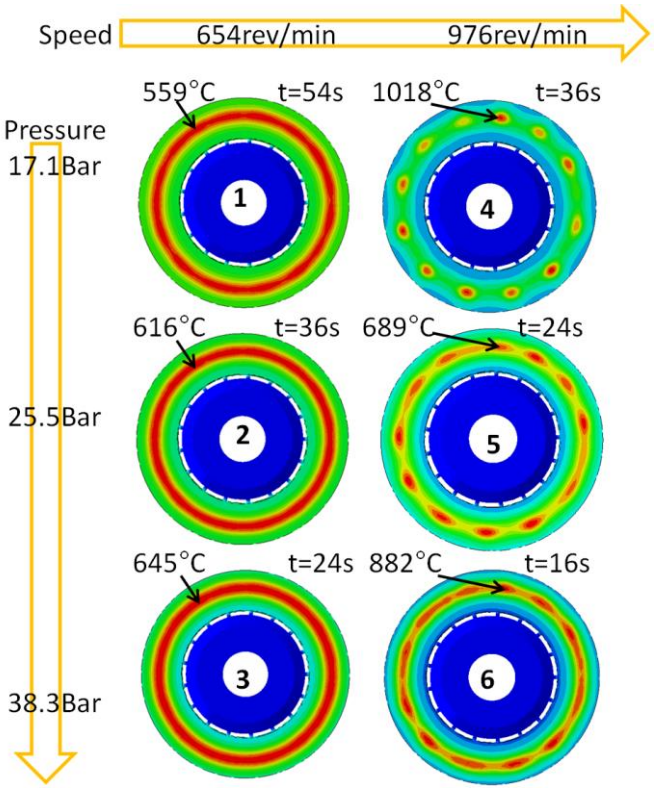

Figure 5.4 Outboard brake disc surface hot spot distribution and maximum brake disc temperature (indicated on figure) of the FE models with the same energy at different speeds and loads

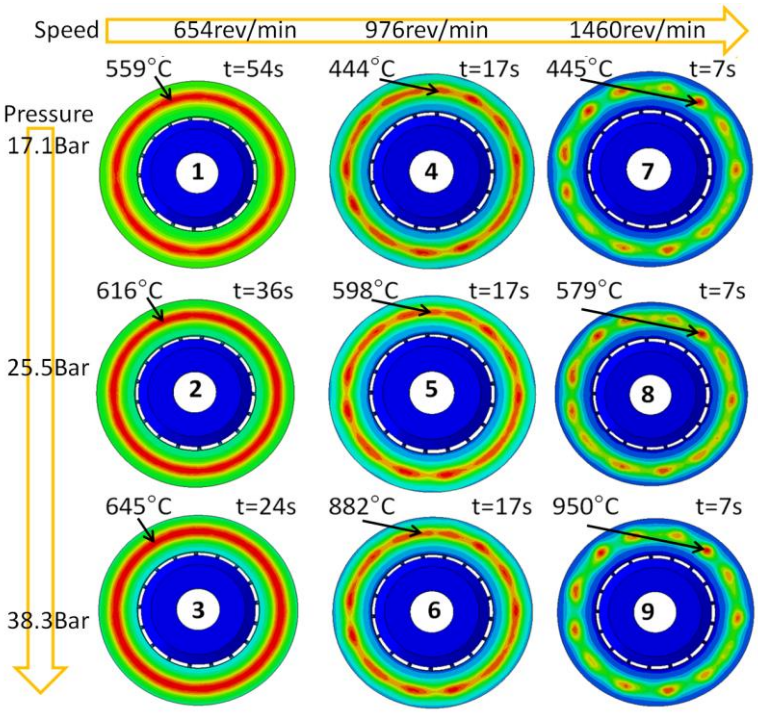

Figure 5.5 Brake disc outboard surfaces temperature distribution and maximum temperature (indicated on figure) of the FE models at the moment that hot spots appeared at different speeds and loads

5.3 Effects of pins on hot spotting

In previous works, it was found that the number of pins in a two piece brake disc correlated with the number of hot spots [1, 12, 16]. As an extension of this work, two possible structural perturbations that the pins can provide to trigger hot spots: periodic constraints and periodic variation of thermal mass were investigated by modifying the elasticity and specific heat capacity of the pins. Both properties were varied within 80% to 120% in this parametric study. Thus both the main effects and interactions of the properties to the maximum hot spot temperature were identified as showed by Figure 5.6 (left). In general, the 3D plot show that the maximum hot spot temperature varied from 690°C to 730°C in various combinations of Young's modulus and heat capacity. The main effects of both material properties were not linear since the temperature can be either increase or decrease by increasing or decreasing both properties. It illustrated that there was a significant interaction between both properties in terms of maximum hot spot temperature. Regarding the average outboard brake disc surface temperature shown in Figure 5.6 (right), an inverse trend of the variation was predicted when compared with the maximum temperature plot (left). However, the average surface temperature variation was only within 2°C which is insignificant when compared with the maximum hot spot temperature variation of ~40°C. Therefore, for pin material selections, it was important to consider such main effects and interactions to achieve a proper combination for lowering the brake disc temperature. It should be noted that the number of hot spots generated was always 17 in this parametric study.

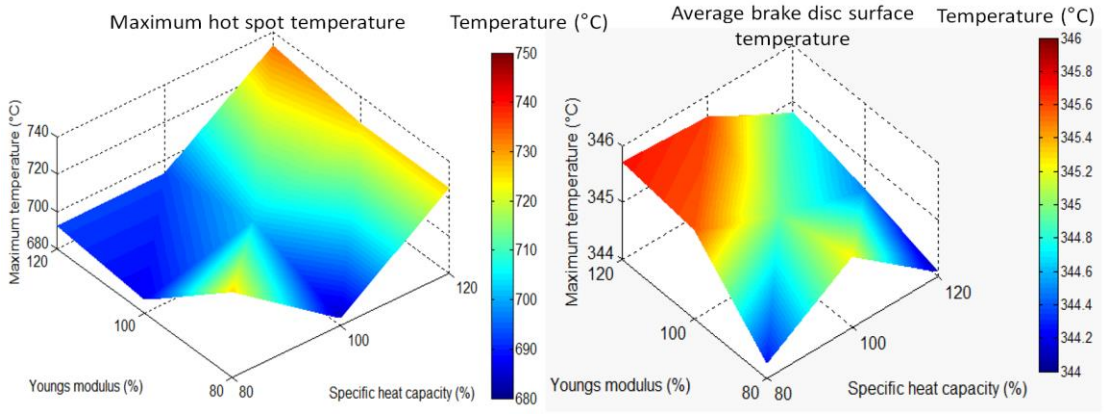

Figure 5.6 Surface plot of the variation of maximum hot spot temperature (left) and average outboard brake disc surface (right) from the FE model with differing Young's modulus and specific heat capacity of the pins (100% = 210GPa and 500J/kg.K)

In addition, a comparison between a two-piece pin mounted brake disc and single piece brake disc with the top hat directly connected to the brake disc was made using a solid brake disc to remove the effects of the vents. Figure 5.7 shows the hot spot distribution at for both models. It illustrates that the number of hot spots was identical for both models, but the location, shape and temperature were different. The hot spots were localised at the outer radius in the single piece brake disc model; this implied that the coning effects of the brake disc toward outboard direction and the subsequent shift of outboard contact zone toward outer radius were affecting the hot spots. Meanwhile, the results of the pin mounted brake disc showed that the hot spots were localised at the mean rubbing radius which reflected an important purpose for implementing pins in

reducing the coning effects. In addition, for the single piece brake disc, the maximum temperature was 799°C and the hot spots were circular, compared with 689°C and ellipse hot spots for the pin mounted brake disc. The different shape and temperature of the hot spots revealed the importance of the top hat and its connection with brake disc in hot spot simulations.

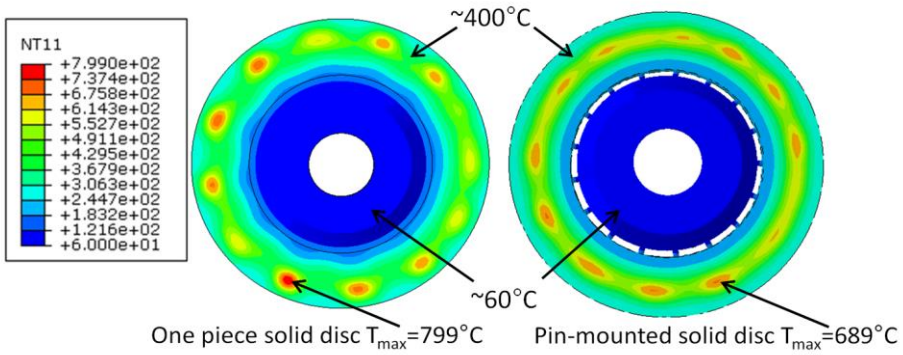

Figure 5.7 FE results of the outboard surface temperature distribution (°C) of a single piece solid brake disc and pin mounted solid brake disc at 24s

5.4 Effects of initial brake disc run-out

Since the relationship between lower order brake disc waviness (run-out) with hot spotting has rarely been focused on in the previous literature, a 2nd order initial brake disc run-out was introduced to investigate its influence on hot spotting. The introduced run-out was much greater than the common values (less than 50 µm) in order to provide more apparent comparisons. Figure 5.8 shows the relative displacement of the mean radii of the brake disc inboard surface (IBM) and outboard surface (OBM) after 24s with, and without, initial 2nd order run-out introduced. The magnitude of the initial run-out for both OBM and IBM are also shown in Figure 5.8 (note there was no change in run-out for the model with no initial run-out). The results illustrated that without initial waviness, the brake disc thickness increased to 100µm with 200µm of coning toward the outboard direction. Regarding the brake disc with initial waviness, ± 200µm 2nd order run-out was introduced with no initial coning. After the braking event, both the inboard and outboard run-out significantly increased to 800µm. Meanwhile, the brake disc thickness growth was less than 100µm and the coning toward the outboard direction was ~200µm.

According to Figure 5.9, only the 2nd order hot spots can be clearly observed in the initial waviness model whereas the 17th order hot spots were developed in the standard model. Therefore, it is clear that the lower order brake disc deformation was triggered by the introduced brake disc initial waviness, and the thermal gradients of hot spots were significantly affected by the brake disc run-out. Under the interference of the brake disc run-out, the heat was not evenly generated throughout the hot spots. It should be noted that, in a real brake disc, it is difficult to develop such a high run-out and the energy distribution between hot spots would be more even as shown in Figure 4.7.

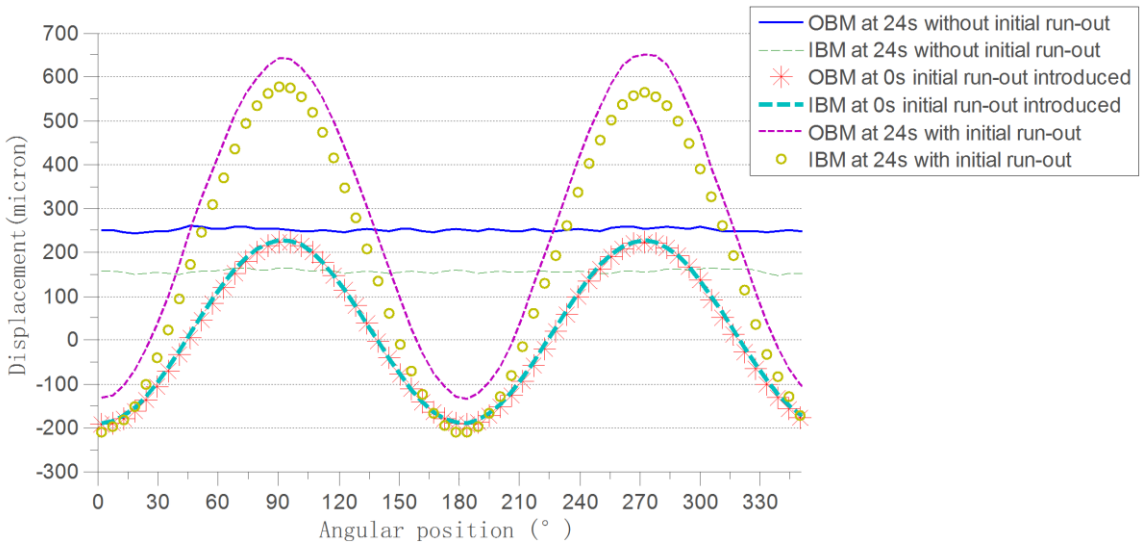

Figure 5.8 FE results showing the relative displacement of brake disc inboard and outboard surfaces with and without initial 2nd order brake disc run-out before (0s) and after (24s) the braking application

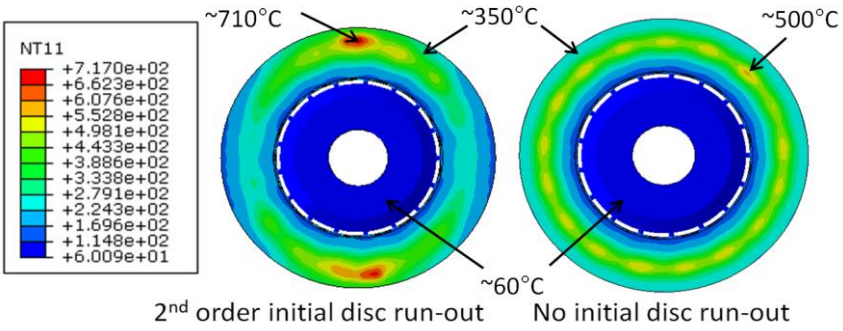

Figure 5.9 FE results showing the outboard brake disc surface temperature distribution (°C) with (left) and without (right) initial run-out

5.5 Effects of brake pad length

According to [18], brake pad length is an important determinant for hot spotting. In the current study, several brake pad arc length (22.5°, 30° and 45°) models were simulated using the axisymmetric model and compared with the standard brake pad length (30°) results. The brake pad length was reproduced by modifying the scale factor discussed in section 3. The results are shown in Figure 5.10, which shows the comparison of temperature distribution for both solid and ventilated brake discs. It can be seen that the maximum brake disc temperature increased with the increase of brake pad length. For brake pads shorter than 36°, no hot spots were developed. This can be explained by the theory of [18] that when the effective brake pad length was shorter than the minimum wavelength of the hot spots or significant geometry perturbation, it is difficult to generate hot spots. This is because the brake pad is not always located at the regions where there is high contact pressure (high spots), therefore each hot spot will receive less energy input. In the axisymmetric model, the material properties are less stiff for the shorter pad, and therefore the contact pressure will be more uniform also resulting in lower energy input per hot spot location. On the contrary, for brake pad length

models greater than 30°, the hot spots appeared and the number subsequently decreased with increasing brake pad length. Moreover, the shape of the hot spots changed from ellipse to circular when the brake pad length was 45°.

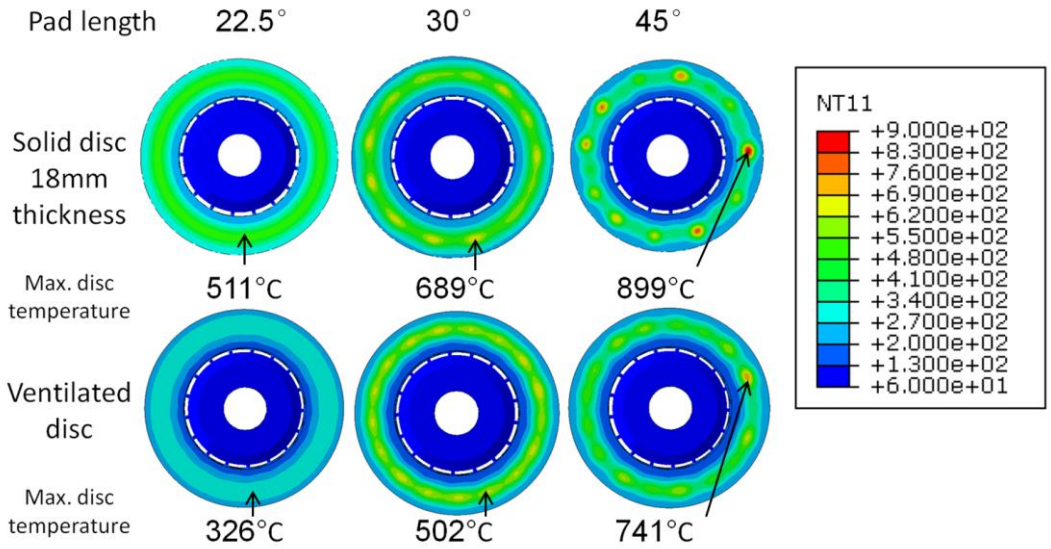

Figure 5.10 FE results showing the hot spot distribution and outboard brake disc surface maximum temperature (°C) for both solid (top) and ventilated (bottom) brake discs at 24s with differing brake pad lengths.

Regarding the solid brake discs, 12 and 6 hot spots were developed for the 30°and 45° models respectively. However, for ventilated brake discs, 17 and 15 hot spots were developed respectively but the maximum brake disc temperatures were lower. In general, the results were in agreement with literature [9, 18, 19] that argued the longer brake pad could develop fewer hot spots.

6 Discussions and conclusions

6.1 Advantage of the axisymmetric brake pad method

According to the TEI theory [4, 5], hot spotting is a thermal localisation phenomenon due to uneven contact pressure and subsequent uneven temperature and displacement distribution. Though the initial hot spotting generation mechanism has been explained in different theories, a subsequent thermal localisation process was also agreed upon [1, 11, 19]. The established 3D FE model incorporating axisymmetric assumptions applied to a 3D brake pad successfully predicted the hot spotting of a ventilated brake disc since it reproduced such a thermal localisation process. Initially, as the brake pad had been modelled and thermo-mechanical contact was considered, the generation of the uneven contact pressure distribution due to uneven deformation was achieved. Moreover, the frictional heat generation was defined by a user-subroutine which enabled the uneven heat generation due to uneven contact pressure distribution. In addition, the uneven heat flux went into the brake disc with a periodic structure. The implementation of the coupled thermal displacement element enabled the uneven deformation due to the uneven temperature and brake disc geometry. Furthermore, as the whole brake disc has been considered the model has the capability to investigate the substructure such as top-hat, pins, vents, and brake disc bulk deformation. Therefore,

the hot spotting prediction for complex brake disc structures is the most significant advantage of the 3D FE model incorporating axisymmetric assumptions applied to a 3D brake pad.

In addition, computing time reduction is a main challenge in hot spot simulations. This is because of the complex rotational friction behaviour calculation. Through the simplification of axisymmetric brake pad and stationary brake disc and brake pad, the computing efficiency can be significantly improved according to Table 3.2. The prediction accuracy of such a method was also verified in section 3. However, due to the limitation of computing power, the capability of hot spotting prediction can only be validated by experiment data i.e. 3D hot spotting simulations under different assumptions (rotating brake disc or real length brake pad) cannot be performed and compared.

In previous experimental works [4, 8], hot spotting investigations were mainly focused on deceleration events. Therefore, there was a debate about the trigger condition of hot spotting – critical speed or energy. However, in this paper, the drag brake applications under various constant speed, pressure and duration were performed, which enabled the comparison of identical energy, duration, and hot spotting generation time.

6.2 Energy, speed and hot spotting

For the parametric studies, there were two interesting phenomena found:

i. Initial brake disc run-out triggered excessive lower order brake disc distortions which resulting significant hot spotting magnitude variation along the brake disc circumference.

ii. At the same energy level, the hot spot number increased as the maximum temperature reduced.

Such observations implied that the energy or heat flux distribution along the brake disc circumference is significant in hot spot generation and the brake disc geometric structure determined the distribution of energy or heat flux.

The hot spot thermal gradient variation with brake disc run-out can be explained by Figure 6.1. The x and z represent the circumferential and axial coordinates of the hot spots and brake disc run-out. The heights of hot spots A and B are Δz_A=z2-z1, Δz_B=z4-z3 and thermal gradients are ΔT_A=T2-T1, ΔT_B=T4-T3 respectively. According to the TEI theory [3, 4, 5], the growth of temperature with the increase of axial brake disc deformation (or contact pressure) is non-linear. Therefore, the thermal gradient ΔT_B of the hot spot B which is closer to the crest of the run-out is greater than ΔT_A, if the heights of hot spots are equal ($\Delta z_A = \Delta z_B$).

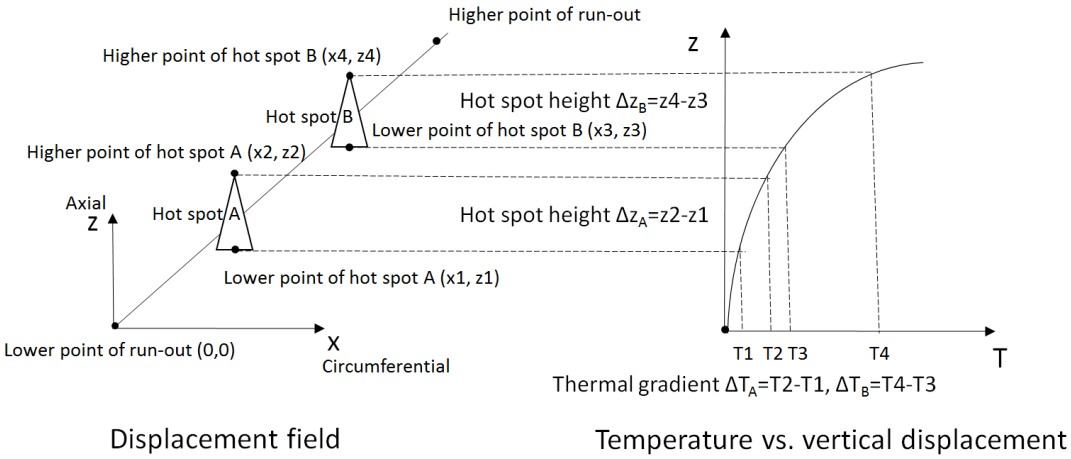

Figure 6.1 Effects of brake disc run-out on the thermal gradients of hot spots

According to the parametric study of different speed and pressure, the speed was more important on the hot spot generation time and distribution than the pressure and total energy input. This was agreed by the TEI theory [3, 4, 5] that the critical speed was the trigger of hot spotting. In addition, the load had no effect on the hot spot distribution but did affect the temperature. This was also agreed by the TEI theory [5] that the initial contact pressure does not affect the pressure variation. At the same energy level but different braking power, both speed and pressure affect the hot spot distribution and magnitude. However, the speed was the predominant factor. This revealed that the ratio between speed and pressure was the determinant of hot spotting rather than the total energy level in such a model. However, it should be noted that as observed in Figures 5.3-5.5, for a given constant braking power, the energy level or the brake duration also act a determinant of hot spot distribution. Therefore, it is suggested that a systemic experiment should be performed on drag brake condition for a solid brake disc to validate the observation of the simulations.

6.3 Brake disc waviness and local thermal buckling

It is clear that the waviness, or run-out magnitude of the brake disc grew (Figure 5.8) and that this may influence the hot spot distribution (Figure 5.9). The thermal buckling theory [1, 13, 14] explained the brake disc waviness as a result of the higher order brake disc thermal buckling, and the hot spotting as the subsequent thermal localisations on the peaks of the waviness. Due to the restrictions of the brake disc thermal expansion in the circumferential direction, the circumferential thermal stress will exceed the critical buckling stress of the brake disc plate when a critical temperature is reached. Pin mounted brake discs go some way to alleviate this by permitting radial movement, but do not completely eliminate the problem. However, the previous analytical higher order thermal buckling predictions [13] overestimated the bulk temperature to achieve such waviness. This is due to the fact that the temperature field of the brake disc is highly non-linear in all directions in the transient hot spotting process, rather than uniform temperature distribution as assumed in analytical studies. In addition, the comparison between solid and ventilated brake disc showed that that more hot spots were developed on the ventilated brake disc than the solid brake disc which reflected that the complexity of hot spotting cannot be explained by the thermal buckling theory alone with was agreed by [14]. Although the bulk brake disc temperature is generally

not enough to trigger the higher order bulk thermal buckling [14], the complex constraints applied by the brake disc vanes and pins combined with surface heating may be sufficient to generate localised buckling. Therefore, the actual thermal buckling is more likely to occur locally such as a thin effective buckling layer on the brake disc surface from a periodic section of a ventilated brake disc.

6.4 Cause-effect chain

From the above observations and discussions, a cause-effect chain is provided in Figure 6.2. Three input scenarios were considered: relative low speed (or high speed but the brake duration was short and the energy input was low), moderate speed or energy level, and relative high speed (or medium speed but the brake duration is relative long which gives high energy level). The parametric studies implied that initial waviness, uneven cooling, pin and vent structure can predominantly affect the hot spot distribution when the total energy level or speed were in a moderate range. It will generate the higher order brake disc waviness (17^{th} order in this study) due to localised thermal buckling and the corresponding hot spots will be developed on the peaks of the waviness. At relative high speed/energy, the effects of the periodic structural factors had minor effects due to more excessive distortions and thermal stress. Then, relative bulk brake disc buckling will occur and greater wavelength will be developed in terms of the brake disc waviness, and the macroscopic hot spots will be formulated at the peaks of the waviness due to thermal localisation effects. Moreover, at relative low speed or energy level, no thermal buckling will happen since the thermal stress was not sufficient to trigger the brake disc waviness buckling even in a small periodic section of a ventilated brake disc. And there will be no subsequent hot spotting due to the small circumferential thermal gradients. However, it is still possible to develop the hot banding phenomenon. This is because of the uneven radial heat generation due to different linear velocity on different brake disc radii and the subsequent thermal localisation amplified these radial temperature gradients into hot bands.

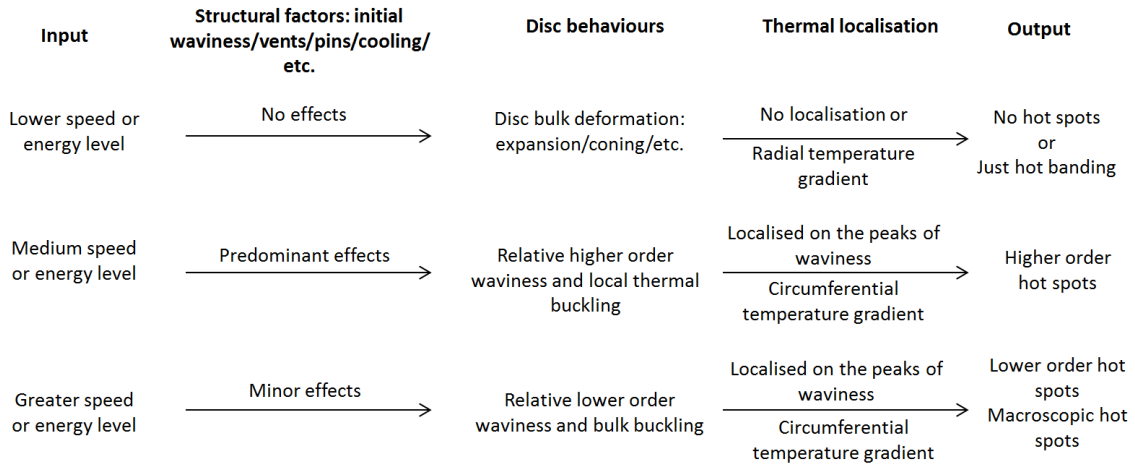

Figure 6.2 Cause effect chains of hot spotting

6.5 Conclusions

Based on the results and discussions, following conclusions are drawn:

i. The axisymmetric brake pad assumption by applying the scaling factor can provide acceptable temperature and displacement field prediction when compared with real brake pad geometry and a rotating brake disc model. The computing efficiency was significantly improved by incorporating both the axisymmetric brake pad (remove the periodic heating) and subroutine (removed the brake disc rotation) i.e. converting the transient problem into quasi-static problem.

ii. The periodic substructure of the ventilated brake disc such as pins and vents can affect the temperature distribution and therefore develop different hot spot characteristics when compared with a solid brake disc with identical effective rotor thickness. The brake disc pins affected the hot spot magnitude in the present case study, yet it was the vents which affected the number of hot spots.

iii. Both speed and energy level were the determinants of hot spots. In terms of hot spot trigger condition, the speed determined the time of occurrence and hot spot distribution. Then, the continuous energy input can change the hot spot distribution and magnitude which reveals the importance of brake duration and total energy input. The result also implies that at the same energy level but different speed, the hot spotting characteristic might not be identical.

iv. The gradients of hot spot temperature and height can be affected by the brake disc run-out due to the non-linear relationship between local deformation, contact pressure and heat generation.

v. Increasing the brake pad length generated fewer hot spots but the temperature of each hot spot increased.

vi. For completeness, wear, plasticity and temperature dependent properties should be modelled to further the understanding of hot spotting.

Acknowledgements

The authors would like to acknowledge the support from Bentley Motors Ltd.

References

[1] Bryant D, Fieldhouse JD, and Talbot CJ. An investigation of the thermo-elastic and thermo-plastic effects during braking. *International Journal of Vehicle Structure & Systems 2011*; 3(1): 57-72.

[2] Kasem H, Brunel JF, Dufenoy P, Siroux M and Desmet B. Thermal levels and subsurface damage induced by the occurrence of hot spots during high-energy braking. *Wear 2011*; 270 (5/6): 355-364.

[3] Barber JR. Thermoelastic instability in the sliding of conforming solids, *Proc. Royal Soc. 1969*; A.312: 381-394.

[4] Lee KJ and Barber JR. An experimental investigation of frictionally-excited thermoelastic instability in automotive disk brakes under a drag brake application. *Journal of Tribology Transactions of the ASME 1994*; 116(3): 409-414.

[5] Dow TA and Burton RA. Thermoelastic instability of sliding contact in the absence of wear. *Wear 1972*; 19(3):315-328.
[6] Lee K and Brooks FW. Hot spotting and judder phenomena in aluminium drum brakes. *Journal of Tribology 2003*; 125(1): 44-51.
[7] Cho H and Cho C. Prediction of hot spots by correlating finite element analysis and measurement for an automotive disk brake. *Tribology Transactions 2008*; 51(5): 609-620.
[8] Sardá A, Haag M and Winner H. Experimental investigation of hot spots and thermal judder. SAE paper 2008-01-2544, 2008.
[9] Panier S, Dufrenoy P and Weichert D. An experimental investigation of hot spots in railway disc brakes. *Wear 2004*; 256(7/8): 764-773.
[10] Kasem H, Dufrénoy P and Desplanques Y. Relationships between Surface Thermal Gradients and Disc Distortion during Stop-Braking with High Energy Dissipation, *Tribol Lett 2012*; 48: 169-181. doi:10.1007/s11249-012-0003-z.
[11] Kao TK and Richmond JW, Douarre A. Brake disc hot spotting and thermal judder: an experimental and finite element study. *International Journal of Vehicle Design 2000*; 23(3): 276-296.
[12] Fieldhouse JD and Beveridge C. An experimental investigation of hot judder. SAE paper 2001-01-3135, 2001.
[13] Fan XL, and Lippmann H, Elastic-plastic buckling of plates under residual stress, *Advances in Engineering Plasticity and its Applications*. Pergamon Press, Amsterdam, 1996.
[14] Ma C. Thermal buckling of automotive brake disc. PhD thesis; The University of Michigan, Michigan, 2004.
[15] Suryatama D, Stewart JD and Meyland CS. Contact mechanics simulation for hot spots investigation. SAE paper: 2001-01-0035, 2001.
[16] Fieldhouse JD, Bryant D, Crampton A, Talbot CJ and Layfield J. A study of thermal judder on a laboratory dynamometer. SAE paper 2008-01-2542, 2008.
[17] Kao KT, Richmond WJ and Moore WM. The application of predictive techniques to study thermo-elastic instability in braking. SAE paper 942087, 1994.
[18] Lee K and Barber JR, Frictional excited thermoelastic instability in automotive disc brakes. *Journal of Tribology 1993*; 115: 607-614.
[19] Panier S, Dufrenoy P, Brunel JF and Weichert, and. Progressive waviness distortion: a new approach of hot spotting in disc brakes. *Journal of Thermal Stresses 2005*; 28(1): 47-62.
[20] Tirovic M and Sarwar GA, Design synthesis of non-symmetrically loaded high-performance disc brakes Part 2: finite element modelling, *Proceedings of the Institution of Mechanical Engineers, Part F: Journal of Rail and Rapid Transit 2004*; 218: 89-104.
[21] Day AJ, Newcomb TP, The dissipation of frictional energy from the interface of an annular disc brake, *Proceedings of the Institution of Mechanical Engineers, Part D: Journal of Automobile Engineering 1984*; 198(13): 201-209.
[22] Zagrodzki P, Lam KB, Al Bahkali E and Barber, JR. Nonlinear transient behaviour of a sliding system with frictionally excited thermoelastic instability. *Journal of Tribology 2001*; 123: 699-708.
[23] Jung DH, Jung SP and Chung WS. Numerical analysis technique to estimate the reliability of a disc brake system – hot judder simulation. *Applied Mechanics and Materials 2012*; 152-154: 723-726.

[24] Jung SP, Park TW, Lee JH, Kim WH and Chung WS. Finite element analysis of thermalelastic instability of disc brakes. *Proceedings of the World Congress on Engineering 2010 Vol II*; WCE 2010, June 30 - July 2: London, UK.
[25] Loizou A. Modelling and simulation of thermo-mechanical phenomena at the friction interface of a disc brake. PhD thesis; University of Bradford, UK, 2001.
[26] Limpert R. *Brake Design and Safety Third Edition*. SAE. ISBN: 978-0-7680-3438-7, 2011.
[27] Tang JH, Bryant D and Qi HS. A 3D Finite Element Simulation of Ventilated Brake Disc Hot Spotting, *Eurobrake 2016*, June 13- June 15: Milan, Italy; EB2016-SVM-025.
[28] Kasem H, Dufrénoy P and Desplanques Y. Two-/three-dimensional hybrid model of the thermomechanical behaviour of disc brakes, *Proceedings of the Institution of Mechanical Engineers, Part F: Journal of Rail and Rapid Transit 2004*; 218: 17-30.